Proc. of the 8th International Symposium on Geotechnical Safety and Risk (ISGSR)
Edited by Jinsong Huang, D.V. Griffiths, Shui-Hua Jiang, Anna Giacomini and Richard Kelly
 Published by Research Publishing, Singapore.
doi: 10.3850/978-981-18-5182-7_03-009-cd

Application of Image Segmentation for Predicting Slope Failure Mechanism in Spatially Variable Soils

Ze Zhou Wang[1], Jinzhang Zhang[2], Siang Huat Goh[1] and Hongwei Huang[2]

[1]Department of Civil & Environmental Engineering, National University of Singapore, Singapore.
E-mail: wangzz@u.nus.edu (Ze Zhou Wang); gohsianghuat@nus.edu.sg (Siang Huat Goh)
[2]Department of Geotechnical Engineering, Tongji University, China.
E-mail: zhangjz@tongji.edu.cn (Jinzhang Zhang); huanghw@tongji.edu.cn (Hongwei Huang)

Abstract: The representation of the spatial variability of soil properties in the form of random fields permits advanced and realistic probabilistic assessment of slope stability. As the intensity and the spatial distribution of soil properties vary in different random field realizations, the resulting failure mechanisms will also be different. Not only does the location of the failure surface vary, but the failure mode itself could also change. While the random field finite element method (RF-FEM), which adopts the shear strength reduction technique to naturally seek out the failure mechanism, is advantageous over other numerical schemes that need the failure mode to be defined a-priori, it suffers from a lack of computational efficiency. In this paper, the application of the image segmentation technique for predicting slope failure mechanism in spatially variable soils is investigated. The deep learning model based on the Resnet-18 architecture is applied to study the failure mechanism of a soil slope modified from a real case study. With sufficient training samples, the deep learning model can function as an image segmentation tool to delineate the sliding mass and the intact mass in the slope, based on which the mode and the location of the slip surface can be predicted without the need to perform the time-demanding random field finite element analysis. By using such an image segmentation tool, a large number of Monte-Carlo realizations of random fields can be efficiently analyzed. The spatial distribution of failure surfaces and the statistical distribution of sliding volume can then be calculated, leading to an improved understanding of slope reliability.

Keywords: Spatial variability; Slope stability; Failure mechanism; Image segmentation.

1 Introduction

The inherent spatial variability of the physical and mechanical properties of natural soils has been considered as one of the major sources of uncertainties in the geotechnical engineering community (Phoon and Kulhawy 1990; Griffiths et al. 2009; Jiang et al. 2022). In the majority of the slope reliability analyses in spatially variable soils, the safety of the slope is typically characterized by the term "probability of failure (P_f)". Other than the probability of failure, the failure mechanism of the slope also serves as an important source of information for the analysis, design and management of the system. For example, piles are often used to stabilized slopes (Gong et al. 2019). The selection of pile length and location are critically dependent on the failure mechanism of the slope.

Traditional probabilistic slope analysis may not have rigorously investigated the failure mechanism. Studies, such as Cho (2010), and Li et al., (2015), adopted the Limit Equilibrium Method (LEM) and define the failure mode a-priori. In this regard, the random field finite element method (RF-FEM), which adopts the shear strength reduction technique to naturally seek out the critical failure mechanism, is a more rigorous technique. However, many studies typically showed only one or a few selected failure surfaces (Griffiths et al. 2009; Liu et al. 2018), which may not be sufficient for providing a comprehensive understanding of the failure mechanism of the slope.

As the intensity and the spatial distribution of soil properties vary in different random field realizations, not only does the location of the failure surface vary, but the failure mode itself could also change. Van den Eijnden and Hicks (2017), for example, coupled the RF-FEM with subset simulation to investigate the spatial distribution of slope failure surfaces, and showed that the location of the failure surfaces can vary significantly. Furthermore, Chen et al. (2022) investigated both the location and shape of the failure surface using the Monte-Carlo simulation approach. They reported that the failure mode can vary from a shallow failure to a deep-seated failure in different random field realizations. In some cases, progressive failure that involves multiple failure surfaces may also occur.

In order to derive a more complete picture of the failure mechanism of a slope, many random field realizations are needed, which may lead to excessive computational costs. To this end, this paper proposes to use the concept of image segmentation to provide an efficient computational tool to facilitate a comprehensive investigation of slope failure mechanisms in spatially variable soils. Essentially, the failure mechanism of a slope involves a sliding body and an intact body. The surface that delineates the two bodies is treated as the failure surface. In this regard, an image segmentation model can be trained to provide a viable tool to automatically differentiate the sliding mass from the intact mass. With such an image segmentation tool, many Monte-Carlo

realizations of random fields can be efficiently analyzed. The spatial distribution of failure surfaces, failure mode and sliding volume can then be calculated, leading to an improved understanding of the slope reliability.

2 Methodology and Implementation

2.1 Interpreting random fields

In the field of computer science, Convolutional Neural Networks (CNNs) specialize in interpreting data that has a grid-like topology, such as an image. CNNs, through the use of convolutional filters, can extract features of the image taking into account pixel positions and the influence of nearby pixels. A random field, in essence, has a grid-like topology, and can be regarded as an "image" that describes the intensity and the spatial distribution of soil properties. In this regard, it is reasonable to hypothesize that CNNs are capable of interpreting and processing random fields in a similar manner as they are used for images. In fact, interpreting random fields using CNNs have been recently demonstrated to be effective in some studies (Wang and Goh 2021; Wang and Goh 202; Zhang et al., 2021a; Zhang et al., 2021b). Therefore, the feasibility to couple random fields with CNNs lays the foundation of using the image segmentation approach to study slope failure mechanism.

2.2 Image segmentation

Image segmentation involves partitioning an image into several regions or segments based on the characteristics of the pixels in the image. This technique has a wide range of engineering applications, including, but not limited to, medical image analysis, autonomous vehicles, and landslide susceptibility. Figure 1 shows an example of image segmentation task. Based on the characteristics of the pixels, this image is partitioned into several objects. In the literature, numerous algorithms have been developed to perform the task, such as thresholding, k-means clustering, and sparsity-based methods. In the last decade, deep learning-based image segmentation algorithms, which have provided improved performance, have received much research. In this paper, the Deeplab v3+ (Chen et al. 2018), which is based on a convolutional network, is used to perform the image segmentation task.

Figure 1. An example of image segmentation. (www.mathswork.com)

2.3 Implementation procedures

Figure 2 illustrates the procedures for implementing the image segmentation model to study the slope failure mechanism in spatially variable soils. The implementation consists of three parts: (i) data pre-processing, (ii) training of the image segmentation model, and (iii) slope failure mechanism investigation.

2.3.1 Data pre-processing

After generating a random field (e.g. Figure 2 (a)), the shear strength reduction technique can naturally seek out the failure mechanism (e.g. Figure 2(b)). The slope body exhibiting large displacement values is considered as the sliding mass while the remaining slope body is the intact mass. However, it is not trivial to objectively define "large displacement" and draw the failure surface. To this end, the k-means clustering technique is used to automatically and objectively separate the displacement field into the two bodies (Van den Eijnden and Hicks, 2017), and a clear failure surface can be identified (e.g., Figure 2 (c)). In a nutshell, the image shown in Figure 2 (a) is the image to be segmented while the image shown in Figure 2 (c) shows the results of the segmentation. The procedures are then repeated for X different input random fields, and this concludes the data pre-processing part.

2.3.2 Training of the deep-learning model

The X pairs of input random fields and the segmentation results (e.g. Figure 2 (c)) are then adopted as the training data of the image segmentation model. The Deeplab v3+ and the weights initialized from the pre-trained Resnet-18 network are used in the present study. Due to the complexity of the model, the architecture is not shown. Details pertaining to the architecture of the model can be found in Chen et al. (2018). Other details pertaining to the hyperparameter values, and the training process will be elaborated in the subsequent parts of this paper.

2.3.3 Slope failure mechanism

After sufficient training, the image segmentation model gains the capability to partition the slope into the sliding body and the intact body without running the RFEM model. In this regard, a large set of random field samples can then be generated, and the segmentation results can be efficiently predicted using the trained model without having to perform the finite element analyses. After obtaining the failure surfaces associated with a sufficiently large set of random fields, the spatial distribution of the failure surfaces and the failure modes can be investigated.

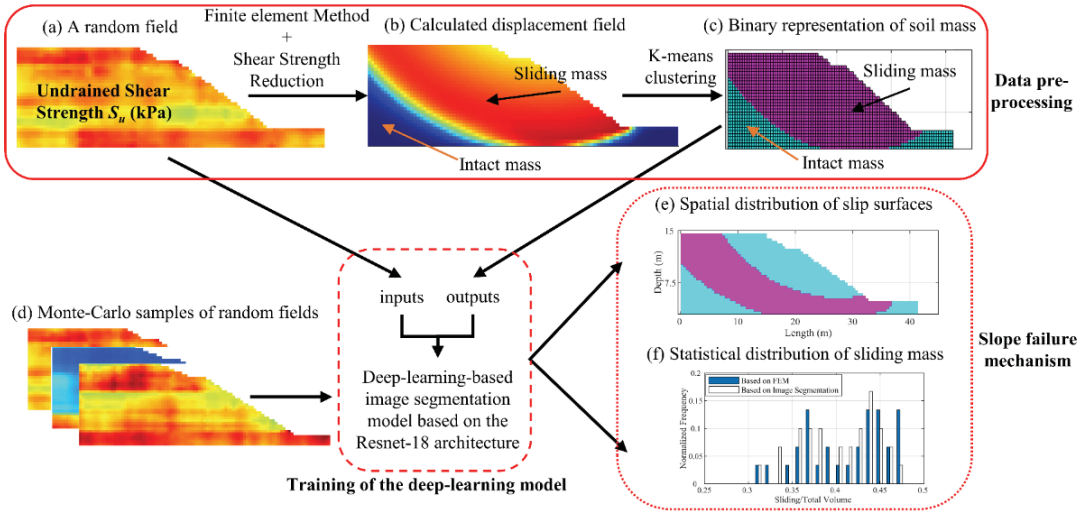

Figure 2. Implementation procedures.

As shown in Figure 2 (e), the failure surfaces obtained from many random field realizations can be co-plotted in a figure. The mode, size, and location of the failure surfaces can be visualized, and the extent of the area covered by the failure surfaces can also be investigated. In addition, the sliding volume, which is key information in landslide mitigation, can also be efficiently calculated, e.g. Figure 2 (f).

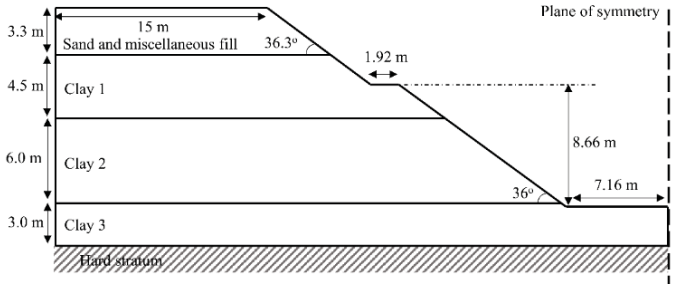

Figure 3. Geometry and geological profile of Congress Street cut.

3 Illustrative Example

In this section, the application of the image segmentation model is illustrated using a slope example modified from a real case history, namely the Congress Street cut at Chicago (Wang and Goh 2021a). The failure mechanism and the sliding volume predicted using the trained image segmentation model will be validated by comparing against the benchmark RF-FEM predictions.

3.1 Description

Figure 3 shows the details of the example, and Table 1 shows the statistics of the material parameters. The fill layer is statistically homogeneous while the three clay layers are each characterized using spatially variable undrained shear strength S_u. The commercial finite element software Optum G2 is used to perform the strength-reduction calculations to obtain the displacement field. The Karhunen-Loève expansion with 1000 terms and a single exponential autocorrelation function is used to generate random fields within the Optum G2 software. The discretization error is approximately 2 x 10^{-6}, which satisfies the requirement suggested by Huang et al. (2013) (i.e., 10^{-5}). To validate the results of the image segmentation model, a direct Monte-Carlo Simulation (MCS) run comprising finite element analyses of the 100,000 random field samples is first performed using Optum G2. In

this regard, the failure mechanism predicted using the image segmentation model will be compared with the benchmark results obtained using the RFEM model. Table 2 summarizes key information of the model.

Table 1. Statistics of the material parameters considered in the illustrative example (Wang and Goh 2021b)

Layers	Unit Weight (kN/m^3)	Friction angle ϕ (°)	Undrained Shear Strength S_u (kPa)			Scale of fluctuation (SoF)	
			Mean	CoV	Distribution	SoF_h (m)	SoF_v (m)
Sand	21	30					
Clay 1	19.5	-	85	0.25	Lognormal	35	10
Clay 2	19.5	-	70	0.19	Lognormal	35	10
Clay 3	20	-	80	0.20	Lognormal	35	10

Table 2. Configurable hyper-parameters of the image segmentation model

Solver	Learning rate	Minimum batch size	L2 regularization rate
Stochastic gradient descent	0.01	16	0.001

3.2 Results interpretation

Following the implementation procedures outlined in Section 2.3, 500 pairs of random fields and segmentation results are generated as the training dataset. Another 250 pairs of data are then generated as the validation dataset. Figure 4 shows the typical training and validation processes. The accuracy calculations, which are evaluated based on a pixel-wise comparison between the predicted and the true results, indicate that the deep learning image segmentation model is reasonably trained (~97% accuracy).

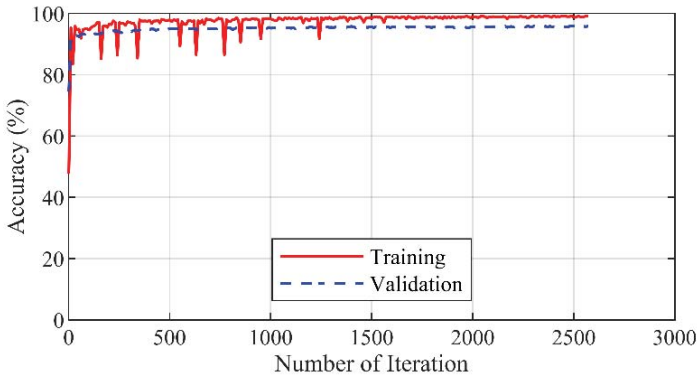

Figure 4. Typical training and validation accuracy.

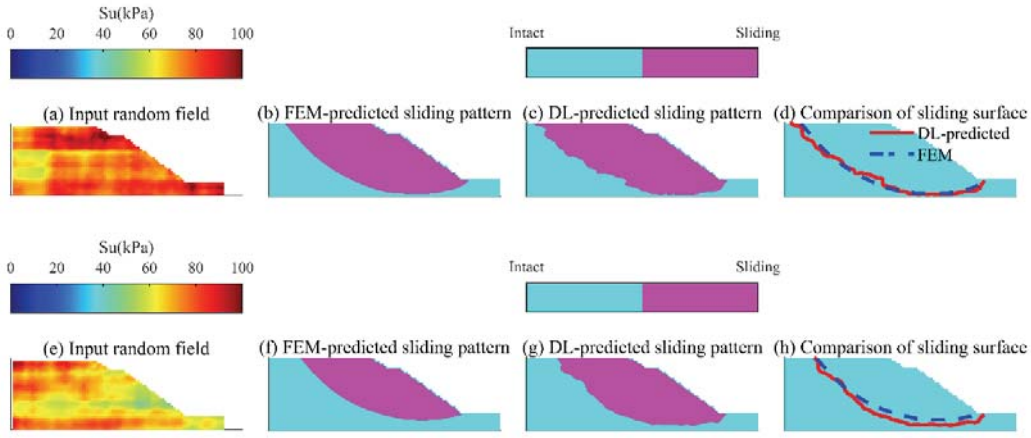

Figure 5. Comparison of failure mechanisms predicted using FEM model and the trained image segmentation model.

Figure 5 compares the failure mechanism predicted using the FEM model and the image segmentation model for two selected realizations. The input random fields are shown in Figures 5 (a) and (e), and the associated FEM calculated failure mechanisms are shown in Figures 5 (b) and (f). A deep-seated failure mode is observed in Figure 5 (b) while a shallow failure mode is seen in Figure 5 (f). As shown in Figures 5 (c) and (g), the image segmentation model reasonably identifies the sliding mass and the intact mass for the two selected realizations although the boundary is not as smooth as that predicted using the FEM model. The failure surfaces

obtained using the FEM model and the image segmentation model are co-plotted in Figures 5 (d) and (h); the good agreement between the two sets of results indicate that the image segmentation model is effective in predicting the failure mechanism.

Figure 6 compiles the failure surfaces (e.g. Figure 5 (d)) associated with all the random fields. In this way, it is possible to visualize the extent of the area covered by the failure surfaces. With reference to Figure 6 (b), the failure surfaces can vary significantly in a spatial manner and cover a quite large area of the slope. While a deep-seated failure mechanism can be obtained in some realizations, the slope can also fail following a shallow failure mode. In this regard, it is necessary to run enough realizations for a rigorous evaluation of the failure mechanism.

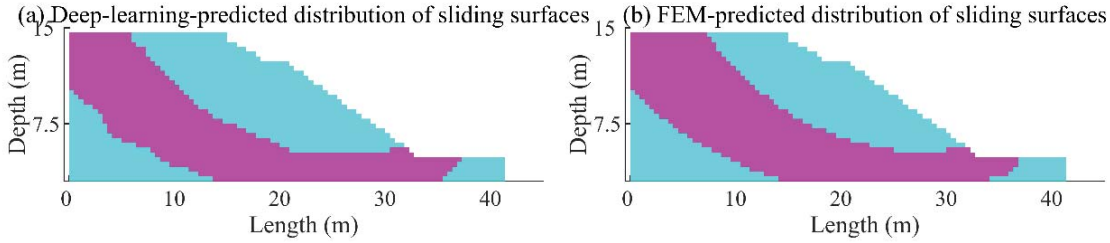

Figure 6. Spatial distribution of failure surfaces predicted by (a) the image segmentation model, and (b) FEM model.

Figure 6 (a) shows the predictions made using the image segmentation model. By visual inspection, the spatial distribution of the failure surfaces is reasonably predicted. Similar to the results shown in Figure 5 (c), although the boundary is not very smooth, both the deep-seated and the shallow failure modes are reasonably predicted. A matching rate index (MR), defined as follows (Zhang et al. 2022), is used to quantify the accuracy.

$$MR(k) = \frac{TP + TN}{TP + FP + TN + FN} \tag{1}$$

where *TP* is the total number pixels where the image segmentation model correctly labels as failure surfaces; *FP* refers to the number of pixels where the model wrongly labels as failure surfaces; *TN* then represents the total number of pixels where the model correctly identifies as non-failure surfaces; and *FN* is the number of pixels where it wrongly identifies as non-failure surfaces. According to Eq. (1), the image segmentation model achieves a matching rate of 0.938 (93.8%), signifying that the model is highly accurate in predicting the failure mechanism of the slope under study.

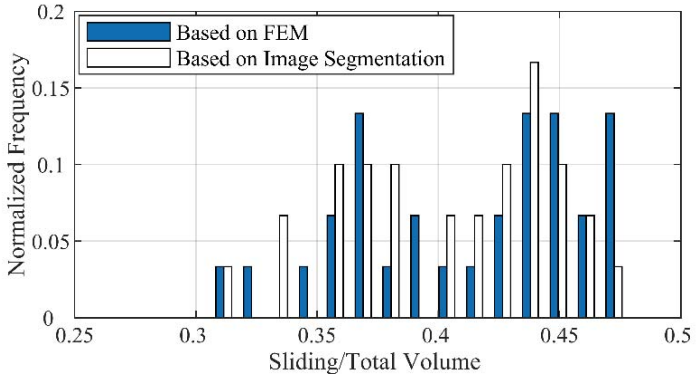

Figure 7. Comparison of the normalized sliding volume predicted using FEM model and the image segmentation model.

Last, Figure 7 compares the normalized sliding volume predicted using FEM model and the image segmentation model. The normalized sliding volume refers to the percentage of the total volume that belongs to the sliding body. In general, the normalized sliding mass ranges from 30% to 50%, which provides key information for failure mitigation. By visual inspection, the histogram representing the results of the image segmentation model reasonably agrees with the benchmark results obtained using the FEM model, which further confirms the accuracy of the image segmentation model.

4 Discussions and Conclusions

There are some limitations associated with the present study. The definition of the failure mechanism is simplified as the pattern and location of the failure surface. Some aspects of the failure mechanism, e.g., the velocity field and stress-deformation distribution of the slope, are not predicted using the deep-learning technique. Further research is warranted. In addition, additional parametric studies are needed to understand the impact of the random field parameters, e.g., scale of fluctuation, on the slope failure mechanism.

In conclusion, this paper presents an efficient deep learning-based image segmentation model to predict the failure mechanism of a slope in spatially variable soils. The image segmentation model can facilitate a rigorous investigation of the slope failure mechanism without incurring the high computational cost required by the Monte-Carlo simulation and the random field finite element analysis. While this paper provides a preliminary investigation on the use of image segmentation technique to facilitate the random field finite element analysis, additional studies pertaining to the influence of the training sample size and the applicability of the method in handling multiple cross-correlated random fields are warranted. Major conclusions are drawn as follows:

(i) The concept of using the image segmentation technique to facilitate the slope failure mechanism investigation in spatially variable soils is effectively validated.

(ii) The proposed image segmentation model successfully delineates the sliding mass and the intact mass. With a matching rate of 93.8%, the spatial distribution of the failure surfaces, the failure model and the normalized sliding volume are accurately calculated using the image segmentation model.

Acknowledgments

This work was supported by the National Natural Science Foundation of China (grant Nos. 52130805) and Shanghai Science and Technology Committee Program (No. 20dz1202200). The financial supports are gratefully acknowledged.

References

Cho, S. E. (2010). Probabilistic assessment of slope stability that considers the spatial variability of soil properties. *Journal of Geotechnical and Geoenvironmental Engineering*.

Chen, L. C., Zhu, Y., Papandreou, G., Schroff, F., & Adam, H. (2018). Encoder-decoder with atrous separable convolution for semantic image segmentation. In *Proceedings of the European conference on computer vision (ECCV)* (pp. 801-818).

Chen, L. L., Zhang, W. G., Chen, F. Y., Wang, L., Gu, D. M., Wang, Z. Y. (2022). Probabilistic assessment of slope failure considering anisotropic spatial variability of soil properties. *Geoscience Frontiers*.

Griffiths, D. V., Huang, J., & Fenton, G. A. (2009). Influence of spatial variability on slope reliability using 2-D random fields. *Journal of Geotechnical and Geoenvironmental Engineering*.

Gong, W., Tang, H., Wang, H., Wang, X., & Juang, C. H. (2019). Probabilistic analysis and design of stabilizing piles in slope considering stratigraphic uncertainty. *Engineering Geology*.

Huang, J., Lyamin, A. V., Griffiths, D. V., Krabbenhoft, K., & Sloan, S. W. (2013). Quantitative risk assessment of landslide by limit analysis and random fields. *Computers and Geotechnics*, *53*, 60-67.

Jiang, S. H., & Huang, J. S. (2016). Efficient slope reliability analysis at low-probability levels in spatially variable soils.

Jiang, S. H., Huang, J., Griffiths, D. V., & Deng, Z. P. (2022). Advances in reliability and risk analyses of slopes in spatially variable soils: A state-of-the-art review. *Computers and Geotechnics*, *141*, 104498.

Li, D. Q., Jiang, S. H., Cao, Z. J., Zhou, W., Zhou, C. B., & Zhang, L. M. (2015). A multiple response-surface method for slope reliability analysis considering spatial variability of soil properties. *Engineering Geology*.

Liu, Y., Zhang, W., Zhang, L., Zhu, Z., Hu, J., & Wei, H. (2018). Probabilistic stability analyses of undrained slopes by 3D random fields and finite element methods. *Geoscience Frontiers*.

Phoon, K. K., & Kulhawy, F. H. (1999). Characterization of geotechnical variability. *Canadian geotechnical journal*, *36*(4), 612-624.

Van den Eijnden, A. P., & Hicks, M. A. (2017). Efficient subset simulation for evaluating the modes of improbable slope failure. *Computers and Geotechnics*.

Wang, Z. Z., & Goh, S. H. (2021). Novel approach to efficient slope reliability analysis in spatially variable soils. *Engineering Geology*, *281*, 105989.

Wang, Z. Z., & Goh, S. H. (2022). A maximum entropy method using fractional moments and deep learning for geotechnical reliability analysis. *Acta Geotechnica*, *17*(4), 1147-1166.

Zhang, J., Phoon, K. K., Zhang, D., Huang, H., & Tang, C. (2021a). Deep learning-based evaluation of factor of safety with confidence interval for tunnel deformation in spatially variable soil. *Journal of Rock Mechanics and Geotechnical Engineering*, *13*(6), 1358-1367.

Zhang, J. Z., Zhang, D. M., Huang, H. W., Phoon, K. K., Tang, C., & Li, G. (2021b). Hybrid machine learning model with random field and limited CPT data to quantify horizontal scale of fluctuation of soil spatial variability. *Acta Geotechnica*, 1-17.

Zhang, J. Z., Liu, Z. Q., Zhang, D. M., Huang, H. W., Phoon, K. K., & Xue, Y. D. (2022). Improved coupled Markov chain method for simulating geological uncertainty. *Engineering Geology*, 106539.